

GreedyPixel: Fine-Grained Black-Box Adversarial Attack Via Greedy Algorithm

Hanrui Wang^{1,*}, Ching-Chun Chang¹, Chun-Shien Lu², Christopher Leckie³, and Isao Echizen^{1,4}

¹National Institute of Informatics, Japan ²Academia Sinica, Taiwan

³The University of Melbourne, Australia ⁴The University of Tokyo, Japan

{hanrui_wang, ccchang, iechizen}@nii.ac.jp, lcs@iis.sinica.edu.tw, caleckie@unimelb.edu.au

Abstract—A critical requirement for deep learning models is ensuring their robustness against adversarial attacks. These attacks commonly introduce noticeable perturbations, compromising the visual fidelity of adversarial examples. Another key challenge is that while white-box algorithms can generate effective adversarial perturbations, they require access to the model gradients, limiting their practicality in many real-world scenarios. Existing attack mechanisms struggle to achieve similar efficacy without access to these gradients. In this paper, we introduce *GreedyPixel*, a novel pixel-wise greedy algorithm designed to generate high-quality adversarial examples using only query-based feedback from the target model. GreedyPixel improves computational efficiency in what is typically a brute-force process by perturbing individual pixels in sequence, guided by a pixel-wise priority map. This priority map is constructed by ranking gradients obtained from a surrogate model, providing a structured path for perturbation. Our results demonstrate that GreedyPixel achieves attack success rates comparable to white-box methods without the need for gradient information, and surpasses existing algorithms in black-box settings, offering higher success rates, reduced computational time, and imperceptible perturbations. These findings underscore the advantages of GreedyPixel in terms of attack efficacy, time efficiency, and visual quality.

Index Terms—Adversarial attack, black-box, pixel-wise, greedy algorithm.

1. Introduction

1.1. Background and Motivation

Adversarial attacks have become the predominant methods for assessing the robustness of deep learning models, emphasizing and exploiting the sensitivity of these models to subtle perturbations. These attacks are typically divided into white-box and black-box attacks. White-box attacks assume comprehensive knowledge of the target model, allowing for the utilization of gradient information for direct optimization [8], [11], [15], [18],

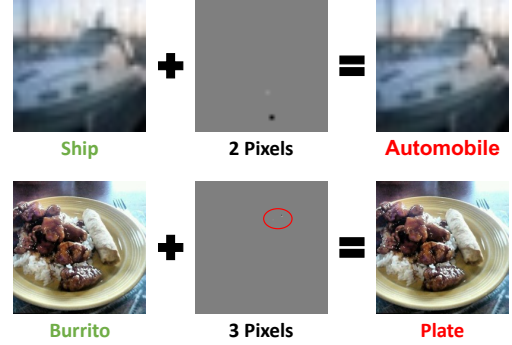


Figure 1. Successful adversarial examples generated by the proposed GreedyPixel method, achieving high visual fidelity by perturbing only a minimal number of pixels without leveraging gradient information from the target model.

[35]. Black-box attacks assume only the output labels or confidence scores (*i.e.*, label- or score-based) and employ various strategies such as submodular searching [2], [37], genetic algorithms [57], [65], learning in the frequency-domain [7], [32], [34], [59], using a local surrogate model [6], [26], [33], [44], [61], or training a generator [16], [28], [29], [67]. In this paper, we focus on adversarial attacks that meet the following requirements.

(i) **Pixel-wise:** Adversarial attacks are often criticized for introducing visible noise that degrades visual quality, as they modify all image pixels [2], [6], [7], [16], [26], [28], [29], [32], [33], [37], [44], [57], [59], [61], [65], [67]. Consequently, pixel-wise and sparse attacks with early-stopping criteria have proven effective in minimizing visible changes [55], [56], as depicted in Figure 1. These methods strategically perturb only a subset of pixels, thereby preserving the overall visual quality while still achieving high attack success rates (ASRs).

(ii) **Score-and-transfer-based:** Given the strong and often impractical assumptions required for white-box attacks, our focus is black-box scenarios. Score-based or transfer-based black-box attacks, however, cannot individually adapt to various scenarios. Score-based attacks, a subset of query-based black-box attacks, use confidence scores from the target model for guidance, which are widely used in applications like face recognition [13], medical diagnosis [30], and multimodality [46]. However, they do not utilize available gradient information [2], [7], [37], [55], [56], [65], making them less efficient in white-box settings. Furthermore, due to their inherently suboptimal algorithms compared to white-box attacks, the

*Corresponding author.

This work was partially supported by JSPS KAKENHI Grants JP21H04907 and JP24H00732, by JST CREST Grants JPMJCR18A6 and JPMJCR20D3 including AIP challenge program, by JST AIP Acceleration Grant JPMJCR24U3, by JST K Program Grant JPMJKP24C2 Japan, and by the project for the development and demonstration of countermeasures against disinformation and misinformation on the Internet with the Ministry of Internal Affairs and Communications of Japan.

TABLE 1. RELATED ADVERSARIAL ATTACKS AND THEIR CHARACTERISTICS.

Attack	Strategy	White-Box	Black-Box	High ASR	Minimal Changes	Direct Optimization
AutoAttack* [11]	Multiple attack integration	✓		✓		✓
APGD* [11]	Gradient-based	✓		✓		✓
FGSM [18]	Gradient-based	✓		✓		✓
PGD [35]	Gradient-based	✓		✓		✓
CW [8]	Gradient-based	✓		✓	✓	✓
GreedyFool [15]	Gradient-based	✓		✓	✓	✓
Square Attack [2]	Random submodular searching		✓	✓		✓
PBA [37]	Smart submodular searching		✓	✓		✓
N -HSA _{LF} [7]	Frequency domain		✓			✓
S ² I-FGSM [32]	Frequency domain	✓	✓			✓
Frequency-Aware [59]	Frequency domain	✓	✓			✓
SSAH [34]	Frequency domain	✓	✓		✓	✓
One-Pixel [55]	Pixel-wise		✓		✓	✓
BruSLe* [56]	Pixel-wise		✓	✓	✓	✓
MF-GA [65]	Genetic algorithm		✓	✓		✓
MGA [57]	Genetic algorithm		✓	✓		✓
DeCoW* [26]	Transferable attack	✓	✓			✓
FIA [61]	Transferable attack	✓	✓			✓
BASES [6]	Query-and-transfer-based	✓	✓	✓		✓
GFCS* [33]	Query-and-transfer-based	✓	✓	✓		✓
SQBA* [44]	Query-and-transfer-based	✓	✓			✓
CG [16]	Generator-based	✓	✓	✓		
DifAttack [28]	Generator-based	✓	✓	✓		
CDMA [29]	Generator-based	✓	✓	✓		
MCG* [67]	Generator-based	✓	✓	✓		
GreedyPixel (Ours)	Query-and-transfer-based Pixel-wise Greedy algorithm	✓	✓	✓	✓	✓

*denotes attacks selected for the evaluation comparison in Section 5.
ASR denotes attack success rate.

attack efficacy of existing methods is typically lower than that of white-box approaches, even when ample time and query resources are available [37], [40], [41].

In contrast, transfer-based attacks create transferable adversarial examples (AEs) using surrogate models, which can be adapted to white-box scenarios by substituting the target model [26], [34], [61]. However, their ASRs are degraded due to the difficulty of improving transferability. To address this, query-and-transfer-based attacks have been developed, generating perturbations using a surrogate model guided by query feedback from the target model [6], [33], [44], thus leveraging the strengths of both approaches.

(iii) Direct optimization: Some adversarial attacks employ a generator [16], [28], [29], [67]. However, direct optimization offers several distinct advantages over generator-based approaches. First, direct optimization is resource-efficient and less complex, facilitating easier implementation. Second, it is customizable and flexible, enabling targeted attacks on specific vulnerabilities. Third, it is applicable across multiple models without requiring retraining for each model. Fourth, the ability to generate attacks immediately is crucial in dynamic environments, where rapid adaptation is necessary. Fifth, direct optimization is more data-efficient, which is particularly important when handling sensitive private data. Finally, it mitigates the risk of overfitting that can occur during generator training.

1.2. Difference from Prior Works

As summarized in Table 1, to the best of our knowledge, no existing algorithm satisfies all of the following

criteria simultaneously: score-and-transfer-based, pixel-wise or sparse, and direct optimization. To address this gap, we propose a novel attack framework using a pixel-wise greedy algorithm, termed *GreedyPixel*. GreedyPixel attack is score-based, leveraging only confidence scores from the target model. It employs direct pixel-wise optimization by iteratively refining individual pixels during each iteration. Furthermore, our approach is transfer-based, as the sequence of pixel processing is governed by a priority map that is learned using a surrogate model. Even in the absence of this priority map, the GreedyPixel algorithm remains feasible; however, it operates with reduced efficiency.

Although brute-force strategies are known to identify universally optimal adversarial perturbations, their application is often limited by substantial computational costs and inefficiencies in query-based methods. In contrast, our GreedyPixel approach renders this brute-force strategy feasible for adversarial attacks by implementing a pixel-wise optimization via a greedy algorithm. This approach differs from previous methods that rely on gradient information, genetic algorithms, or generative models. Despite this, GreedyPixel achieves competitive ASRs compared to state-of-the-art (SOTA) techniques. Therefore, GreedyPixel is the first black-box attack to achieve fine-grained manipulations comparable to white-box attacks. This capability extends beyond fooling classifiers to enabling precise alterations of sensitive entities, such as latent codes in diffusion models. These findings position GreedyPixel as a novel contribution that bridges the precision gap between white-box attacks and the broader applicability of black-box methods, thereby advancing the state of the art in adversarial attack methodologies.

While effective, GreedyPixel demands a higher number of queries and increased computational resources as image resolution grows, making it more suitable for low-resolution images and less efficient for high-resolution tasks. To address these challenges and enhance computational efficiency, we introduce a pixel-wise priority map, which guides and prioritizes pixel modifications. This map ranks pixels based on their importance, determined through gradients derived from a surrogate model. Adjusting higher-ranked pixels leads to more significant alterations in model predictions. Replacing the surrogate model with the target model transforms GreedyPixel into a white-box attack, further improving time and query efficiency by utilizing actual gradient information.

Moreover, GreedyPixel enhances the visual quality of AEs by focusing on robust features, such as sharp edges and intricate patterns, thereby making the perturbed pixels less perceptible compared to background noise.

1.3. Contributions

We evaluate the proposed GreedyPixel across three threat models: (i) white-box attack with a constrained attack budget (*i.e.*, limited perturbation size) that utilizes gradient information from the target models; (ii) black-box attack with a constrained attack budget, relying solely on query feedback; and (iii) black-box attack with an unconstrained attack budget, benchmarked against the SOTA sparse attack [56]. GreedyPixel is evaluated using the CIFAR-10 [24] and ImageNet [1] datasets, with image sizes of 32×32 , 64×64 , and 224×224 . Our evaluation includes comparisons with established white-box and black-box attack methodologies, encompassing gradient-based, query-and-transfer-based, generator-based, and pixel-wise attacks [11], [26], [33], [44], [56], [67].

Our empirical results demonstrate that the GreedyPixel attack achieves comparable ASRs to white-box attacks without relying on gradient information. Furthermore, it surpasses existing black-box attack algorithms, delivering higher ASRs, reduced computational time, and less perceptible perturbations, all while constrained by the same maximum number of queries. These findings highlight GreedyPixel’s superior attack efficacy, time efficiency, and visual quality in comparison to benchmark attacks. In evaluations against adversarial defenses [3], [12], [36], [43], [60], GreedyPixel consistently achieves higher ASRs than all benchmarked white-box and black-box attacks. Additionally, we perform ablation studies on the priority map, surrogate models, query efficiency, and image resolution. The findings reveal that the proposed priority map significantly reduces the number of queries, with further improvements achievable when integrating white-box information.

Our contributions are summarized as follows:

- We introduce GreedyPixel, a novel score-and-transfer-based pixel-wise adversarial attack, successfully implementing a brute-force pixel-wise optimization strategy in practice. We empirically demonstrate that GreedyPixel outperforms existing gradient-based, query-and-transfer-based, generator-based, and pixel-wise attack methods in terms of attack efficacy, time efficiency, and

visual quality, both in the presence and absence of adversarial defenses.

- We introduce a pixel-wise priority map that enhances the efficiency of GreedyPixel by prioritizing pixel perturbations based on their impact as determined by an adversarially trained surrogate model. This approach accelerates the adversarial process, improves attack efficiency, and maintains high visual quality of AEs, making the brute-force strategy feasible in practical applications.

2. Related Work

In this section, we review white-box and black-box attacks, summarizing their characteristics and comparing them with our proposed GreedyPixel in Table 1. We also review adversarial defenses and adversarial training used for surrogate models.

2.1. White-Box Attacks

White-box attacks leverage full knowledge of deep learning models, using gradient information for manipulation. Fast Gradient Signed Method (FGSM) [18] was introduced for quick AE generation in a single step, but often fails to find optimal perturbations. In contrast, Projected Gradient Descent (PGD) [35] extends FGSM iteratively, enhancing ASRs by refining perturbations over multiple steps. Auto-PGD (APGD) [11] further enhances performance by dynamically adjusting step sizes, contrasting with PGD’s fixed step size. Carlini-Wagner (CW) attack [8] excels in visual quality but sacrifices ASR and incurs high computational costs. AutoAttack [11], widely used as a benchmark, integrates multiple attack algorithms including APGD. GreedyFool [15] employs a greedy algorithm to filter pixels through a two-stage, distortion-aware method. In the first stage, it selects the most effective candidate positions for modification by considering both the adversarial gradient and the distortion map to maintain imperceptibility. In the reduction stage, it further eliminates less important points. However, GreedyFool is limited to white-box attacks, as it relies on access to gradient information. In contrast, our proposed GreedyPixel focuses on identifying locally optimal perturbations for each pixel through a greedy brute-force approach, without requiring gradient knowledge.

Despite their efficacy, white-box attacks face limitations in black-box scenarios, where target model gradients are unavailable and non-transferable. Moreover, most white-box attacks modify all image pixels, leading to noticeable differences between generated AEs and original images.

2.2. Black-Box Attacks

Black-box attacks employ diverse strategies to generate AEs against machine learning models. One-Pixel attack [55] modifies just one pixel using differential evolution, while Square attack [2] and Parsimonious black-box attack (PBA) [37] use a submodular search. Genetic algorithms are employed by Microbial Genetic Algorithm (MGA) attack [57] and Genetic Algorithm attack with Multiple Fitness functions (MF-GA)

[65], and Feature Importance-Aware (FIA) attack [61] and Deformation-Constrained Warping (DeCoW) attack [26] enhance AE transferability. Query-and-transfer-based methods like Black-box Attack via Surrogate Ensemble Search (BASES) [6], “Gradient First, Coimage Second” (GFCS) attack [33], and Small-Query Black-Box Attack (SQBA) [44] utilize the gradients from a surrogate model and the target model feedback together. BruSLe attack [56] (named in honor of Bruce Lee) learns sparse perturbations with Bayesian methods. Frequency-domain approaches include Spectrum Simulation Iterative Fast Gradient Sign Method (S^2 I-FGSM) [32], N -HSA_{LF} attack [7] (full name not disclosed), and frequency-aware perturbations [59], which improve attack efficacy but may compromise visual quality and ASRs without appropriate training. The Semantic Similarity Attack on High-frequency Components (SSAH) [34] significantly reduces visual quality degradation. However, its limited transferability results in lower ASRs in black-box attack scenarios. Generative models like Conditional Glow (CG) attack [16], Meta Conditional Generator (MCG) [67] attack, Conditional Diffusion Model Attack (CDMA) [29], and DifAttack [28] leverage disentangled feature spaces to generate AEs.

However, these black-box attacks face several challenges. First, their ASRs are generally lower compared to white-box attacks [2], [7], [26], [32], [34], [37], [44], [55], [59], [61]. Second, these attacks often lack adaptability even when provided with white-box knowledge, limiting their performance improvement in such scenarios [2], [7], [37], [55], [56], [65]. Third, the perturbations they introduce are often more perceptible because they manipulate all image pixels [2], [6], [7], [16], [26], [28], [29], [32], [33], [37], [44], [57], [59], [61], [65], [67]. Lastly, approaches that involve training a generator to produce AEs may exhibit weaknesses compared to direct optimization methods [16], [28], [29], [67], as discussed in Section 1.1. These challenges highlight the potential complexity in developing effective black-box attacks, capable of reliably compromising machine learning models.

2.3. Adversarial Defenses

Existing adversarial defenses are divided into three categories: training-time, test-time, and preemptive. Training-time defenses produce robust deep learning models (also known as adversarially trained models) that classify AEs correctly [12], [14], [18], [19], [45], [51], [52], [60], [63]. Test-time defenses combine detection and purification. Detection models are typically trained on AEs to enable the model to distinguish them from benign inputs [9], [21], [25], [36], [69]. In contrast, adversarial purification aims to purify AEs by eliminating or invalidating perturbations. Earlier studies used image distortion for purification [20], [47], [58]. Lately, more practical approaches generate benign replacements for inputs regardless of whether they are malicious [43], [48]. Preemptive defenses aim to generate robust examples that replace the original images, which are then discarded [17], [38], [50]. These robust examples are more challenging to manipulate and thus resist adversarial attacks.

2.4. Adversarially Trained Models

We review adversarially trained models used as surrogate models, focusing on training-time adversarial defenses to correctly classify AEs. Early methods by Goodfellow *et al.* [18] integrated AEs into training data. Shafahi *et al.* [52] optimized backward-pass computations, while Wong *et al.* [63] used random initialization with FGSM. Schwag *et al.* [51] utilized proxy distributions from generative models. Goyal *et al.* [19] showed generative models augmenting data for robustness. Debenedetti *et al.* [12] recommended vision transformers with specific augmentations. Wang *et al.* [60] used denoising diffusion models for augmentation, and Dong *et al.* [14] introduced preemptive examples into the training process. Peng *et al.* [45] developed a robust model with optimized architecture and advanced blocks. Bartoldson *et al.* [3] developed scaling laws for adversarial robustness, integrating the data quality of generative models to accurately predict robustness of unseen configurations, recommend optimal resource allocations, and identify opportunities to reduce model size.

3. Methodology: GreedyPixel

In this section, we provide a comprehensive description of the proposed GreedyPixel attack methodology. The relevant threat models and formal problem definition are outlined in Sections 3.1 and 3.2, respectively. The GreedyPixel attack begins by constructing a pixel-wise priority map based on a surrogate model, as detailed in Section 3.3. The attack then proceeds sequentially, utilizing query feedback from the target model to select pixels in descending order of priority until the stopping criteria are met. This process is defined as the “Pixel-Wise Greedy Algorithm” in Section 3.4. Finally, the complete algorithmic procedure for the GreedyPixel attack is presented in Section 3.5.

3.1. Threat Model

GreedyPixel is designed for black-box adversarial attacks, but it is also adaptive to white-box attacks when the gradient of the target model is available. In its black-box configuration, GreedyPixel operates by relying on query feedback from the target model, which includes the target label and confidence scores. The order in which pixels are processed is determined through a surrogate model that provides accessible gradient information.

Conversely, the white-box version of GreedyPixel leverages direct access to gradient information from the target model itself. This access enables the surrogate model to be substituted with the target model directly, streamlining the adversarial perturbation generation process. This distinction highlights GreedyPixel’s adaptability across different levels of information access in attacking machine learning models. Notably, only transfer-based attacks using a surrogate model, such as [6], [16], [26], [28], [29], [32], [33], [37], [44], [57], [59], [61], [67] and our method, can be transformed to a white-box version, while other black-box mechanisms [2], [7], [55], [56], [65] cannot be further enhanced even given gradients of the target model.

Additionally, GreedyPixel can operate without constraints on the L_∞ -norm distance, as it is a pixel-wise attack. Notably, only pixel-wise and sparse adversarial attacks, such as the One-Pixel attack [55] and the BruSLe attack [56], are feasible within this threat model.

In summary, GreedyPixel is applicable in the following threat models:

- White-box attack with a constrained L_∞ -norm distance.
- Black-box attack with a constrained L_∞ -norm distance.
- Black-box attack with an unconstrained L_∞ -norm distance.

3.2. Adversary Goal and Loss Function

Adversarial attacks aim to manipulate predictions through subtle perturbations. Let x and y denote the original image and its ground-truth label, respectively, and let x' represent the AE, formulated as:

$$x' = x + \delta, \text{ s.t. } \|\delta\|_\infty \leq \epsilon, \quad (1)$$

where ϵ is the maximum allowable perturbation magnitude. Thus, given a loss function ℓ with respect to x' , the optimization objective in GreedyPixel for achieving misclassification is:

$$x' = \arg \min_{x'} \ell(x'). \quad (2)$$

GreedyPixel utilizes the CW loss function [8] to define its optimization problem. The CW loss is based on the assumption that the most efficient attack is to alter the prediction between the target and highest possible non-target label. For the misclassification scenario, the loss function employed by GreedyPixel is formulated as:

$$\ell(x') = Z(x')_y - \max_{i \neq y} Z(x')_i, \quad (3)$$

where $Z(x')$ represents the logits (pre-softmax activations) of the target model (for brevity, we use Z to refer to the target model), and y and i denote the indices, referring to labels. Specifically, $\ell \geq 0$ indicates a correct classification, while $\ell < 0$ signifies a successful misclassification attack.

3.3. Pixel-Wise Priority Map

The pixel-wise priority map determines the sequence in which pixels are processed by the greedy algorithm. The priority assigned to each pixel reflects its importance in the surrogate model Z_s (hereafter, Z_s is used to denote the surrogate model and the logits of surrogate model interchangeably), assessed through the gradient of the CW loss function ℓ with respect to the input x and the ground-truth label y . This prioritization ensures that altering pixels with higher priorities induces more significant changes in predictions. Moreover, the priority map can be updated periodically, focusing adjustments primarily on a limited set of high-priority pixels, which further enhances the visual quality of AEs, while acknowledging a trade-off in the ASR. As the priority map is generated within a

Algorithm 1 Pixel-Wise Priority Map

Input: Original image x of size $C \times H \times W$ and its ground-truth label y , surrogate model Z_s .

Output: Priority Map $\{(h_i, w_i)\}_{i=1}^{H \times W}$.

- 1: $\ell(x) = Z_s(x)_y - \max_{i \neq y} Z_s(x)_i$ (3)
- 2: $g(c, h, w) = \text{backward}(\ell)$ \triangleright gradient map
- 3: $g'(h, w) = \sum_{c=1}^3 (|g(c, h, w)|)$ \triangleright pixel importance
- 4: $\{(h_i, w_i)\}_{i=1}^{H \times W} = \text{DescendingOrder}(g'(h, w))$
- 5: **return** $\{(h_i, w_i)\}_{i=1}^{H \times W}$

TABLE 2. THE RATIO (%) OF PERTURBATION VALUES (IN TERMS OF THEIR ABSOLUTE VALUES) IN EFFECTIVE AES @ L_∞ -NORM $\epsilon = 4/255$.

Value	CIFAR-10	ImageNet	Average
4/255	70.43	42.23	56.330
3/255	8.40	18.47	13.435
2/255	6.46	13.59	10.025
1/255	6.14	12.51	9.325
0	8.57	13.2	10.885

Bold denotes the largest proportion.

surrogate model, its computation does not incur query costs to the target model.

As depicted in Figure 2, the computation of the priority map involves the following steps:

- *Step 1:* Compute the gradient $g(c, h, w) = \nabla_x \ell(x)$ for each pixel in the surrogate model Z_s , where $c \in [1, 3]$, $h \in [1, H]$, and $w \in [1, W]$ denote the channel, height, and width indices in an RGB image of size $H \times W$, respectively.
- *Step 2:* Calculate the importance of each pixel using $\sum_{c=1}^3 |g(c, h, w)|$.
- *Step 3:* Prioritize pixels based on their importance, assigning higher priority to pixels with larger values.

The complete algorithm for generating the priority map is provided in detail in Algorithm 1.

Utilizing an adversarially trained surrogate model will improve the visual quality of AEs by prioritizing robust features like sharp edges or complex patterns. This approach makes manipulated pixels less distinguishable compared to noise applied to the background. Moreover, substituting the surrogate model with the target model will transform GreedyPixel into a white-box attack, where direct gradient information from the target model is utilized for generating AEs. Without using a surrogate model, the pixels could be processed in a random sequence, but the computational cost would be higher, especially for high-resolution images.

3.4. Pixel-Wise Greedy Algorithm

3.4.1. Fixed-Size Perturbations. Unlike other attack algorithms that introduce continuous perturbation values, our pixel-wise greedy algorithm consistently utilizes the maximum perturbation budget (i.e., $\pm\epsilon$).

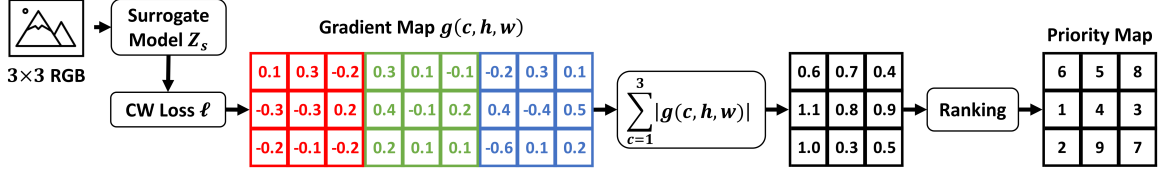


Figure 2. The pixel-wise priority map is constructed by ranking the gradient g of the CW loss function ℓ with respect to the input x and the ground-truth label y in a surrogate model Z_s . Substituting the surrogate model with the target model transforms GreedyPixel into a white-box attack scenario.

As shown in Table 2, we computed the ratio of perturbation values (in terms of their absolute magnitudes) for 1,000 successful AEs generated by AutoAttack [11]. The empirical results reveal that, in successful L_∞ -norm adversarial attacks, perturbations overwhelmingly assume values of $\pm\epsilon$. This finding underscores the pivotal role of these extreme values as the most effective modifications for achieving adversarial success.

Consequently, in GreedyPixel, perturbations for each pixel across all RGB channels are restricted to the set $E = \{-\epsilon, +\epsilon\}$. This targeted approach ensures that GreedyPixel concentrates on perturbations most likely to alter the model’s prediction while strictly complying with the L_∞ -norm constraint.

Although this strategy sacrifices a small fraction of fine-tuned perturbation values, it achieves a lower loss compared to white-box attacks. This improvement can be attributed to GreedyPixel’s ability to mitigate the local-optima challenges inherent in gradient-based methods, as discussed further in Section 3.4.4.

3.4.2. Impractical Brute-Force Attack. Given the finite image size and limited perturbation options, a brute-force attack, in theory, could identify globally optimal perturbations that minimize the CW loss. However, the query cost of such an approach can be expressed as:

$$Q_{BruteForce} = |E|^{H \times W \times C}, \quad (4)$$

where $|E|$ denotes the number of perturbation options, and $H \times W$ represents the image resolution with C channels.

To achieve global optimality with continuous perturbation size options ranging from 0 to the maximum value ($\pm\epsilon$), the computational complexity would escalate to:

$$Q_{BruteForce} = (2 \times \text{int}(\epsilon \cdot 255) + 1)^{H \times W \times C}, \quad (5)$$

where $\text{int}(\epsilon \cdot 255)$ represents the maximum pixel change on a scale from 0 to 255, “2” accounts for \pm , and “+1” includes the value 0.

Even when restricting the brute-force search to maximum fixed-size perturbations ($\pm\epsilon$), the complexity would still remain exponential:

$$Q_{BruteForce} = 2^{H \times W \times C}. \quad (6)$$

This brute-force approach is evidently infeasible due to its exponential computational complexity, rendering global optimization impractical. Consequently, GreedyPixel employs a pixel-wise greedy algorithm to significantly accelerate the optimization process while achieving near-optimal results.

3.4.3. Greedy Strategy. The proposed greedy algorithm for adversarial attacks does not rely on the gradient. Instead, in each iteration, GreedyPixel perturbs a single pixel, replacing its previous perturbation while preserving the perturbations of all other pixels. Therefore, the term “Greedy Algorithm” in our context refers specifically to the pixel-wise perturbation generation process. We are the first to employ this strategy in a manner akin to brute force, which was previously considered computationally impractical. Additionally, we note that a white-box attack [15] utilizing a greedy algorithm refers to the pixel selection process, which differs from the methodology employed in our approach.

Formally, let δ_t represent the perturbation from the previous iteration, which has the same dimensions as the source image x ($H \times W \times C$). At each iteration t , a specific pixel (h_t, w_t) is selected for perturbation. The updated perturbation δ_{t+1} is identical to δ_t except for the pixel at location (h_t, w_t) , where $\delta_t[h_t, w_t]$ is replaced by a new perturbation $\delta_{h_t, w_t} \in \mathbb{R}^{1 \times C}$. This can be expressed as:

$$\delta_{t+1}[h_t, w_t] = \begin{cases} \delta_{h_t, w_t}, & \text{if } (h, w) = (h_t, w_t), \\ \delta_t[h_t, w_t], & \text{otherwise.} \end{cases} \quad (7)$$

The goal is to find the optimal perturbation δ_{h_t, w_t} that minimizes the loss value when added to the input image, as follows:

$$\delta_{h_t, w_t} = \arg \min_{\delta_{h_t, w_t}} \ell(x + \delta_{t+1}), \quad (8)$$

where ℓ refers to Equation (3).

In the proposed localized brute-force approach, GreedyPixel systematically evaluates all eight possible perturbation combinations for δ_{h_t, w_t} , generated from three color channels and two perturbation magnitudes ($E = \{-\epsilon, +\epsilon\}$, $|E|^3 = 8$). The combination that minimizes the loss function is selected, and the resulting optimal perturbation is applied uniformly to the three channels of the target pixel, overwriting any previous modifications.

This iterative, localized search process focuses on perturbing one pixel at a time, incrementally refining the adversarial example. While the search is localized to individual pixels, the accumulation of these fine-grained changes can approximate a globally optimal solution over successive iterations. A detailed description of the complete algorithm is provided in Algorithm 2.

3.4.4. Approximate Optimality. Our greedy strategy applies a “fine-grain” search for AEs, addressing two key limitations found in existing attack algorithms:

Algorithm 2 Greedy Strategy for a Single Pixel

Input: Original image x of size $C \times H \times W$ with $C = 3$, and its ground-truth label y , target model Z , maximum L_∞ -norm magnitude ϵ , selected pixel (h, w) with $1 \leq h \leq H$ and $1 \leq w \leq W$, perturbations δ_t from the previous iteration.

Output: Perturbations δ_{t+1} , loss value ℓ_{t+1} .

```

1:  $\delta_{tmp} \in \mathbb{R}^{8 \times 3}$ ,  $\ell_{tmp} \in \mathbb{R}^8$   $\triangleright$  temporary variables
2:  $\delta_{tmp} = \text{permute}(E = \{-\epsilon, +\epsilon\}, 3)$ 
3: for  $1 \leq i \leq 8$  do
4:    $\delta_{t+1} = \delta_t$ 
5:    $\delta_{t+1}[h, w] = \delta_{tmp}[i]$ 
6:    $\ell_{tmp}[i] = \ell(x + \delta_{t+1})$  (3)
7: end for
8:  $idx = \arg \min \ell_{tmp}$   $\triangleright$  to meet Equation (2)
9:  $\delta_{t+1} = \delta_t$ 
10:  $\delta_{t+1}[h, w] = \delta_{tmp}[idx]$ 
11:  $\ell_{t+1} = \ell_{tmp}[idx]$ 
12: return  $\delta_{t+1}$ ,  $\ell_{t+1}$ 

```

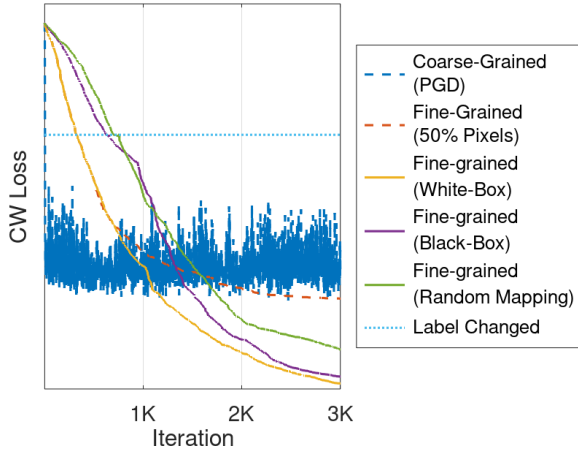


Figure 3. Comparison of the optimality of gradient descent (PGD), partial optimization, and our greedy algorithm. Our “fine-grained” approach achieves lower loss values, indicating improved optimization results relative to other methods. Furthermore, the integration of a priority map and precise gradient information enhances these optimality gains.

Observation 1: Gradient descent in the top-level weights is complicated by the fact that the objective function has many poor local optima [4], [22].

Observation 2: Methods based on partial optimization (e.g., coordinate descent) generally do not guarantee global optimality and may converge to suboptimal points due to the non-convex nature of many optimization problems [37], [40], [41].

These two observations indicate that both the “coarse-grained” gradient-descent approach used in white-box attacks and the partial optimization employed in black-box attacks (even when using “fine-grained” through pixel-wise processing) are unlikely to achieve global convergence. Gradient-based algorithms are more susceptible to converging to suboptimal local minima in non-convex, high-dimensional optimization problems, such as those encountered in deep neural networks. Greedy algorithms, on the other hand, do not rely on gradient information. Instead, they make decisions based on immediate gains at each step, which helps avoid being trapped in local minima.

While it is analytically intractable to derive probabilities of finding the global optimum due to the high dimensionality of both input images and neural networks, we provide experimental evidence in Figure 3 to demonstrate the superior optimality achieved by our approach. Figure 3 demonstrates that while all strategies successfully alter the labels, our “fine-grained” greedy algorithm achieves lower loss values than the other methods by avoiding the local maxima where alternative approaches become trapped, indicating superior optimization.

Compared with black-box attacks, GreedyPixel represents the first black-box attack capable of achieving fine-grained manipulations comparable with white-box attacks, thereby outperforming existing black-box algorithms. This superiority arises from its ability to explore a substantially larger solution space, made feasible with an acceptable computational cost, owing to the proposed priority map. For example, compared to the SOTA black-box pixel-wise BruSLe attack [56], GreedyPixel operates within a solution space of $2^{3 \times H \times W}$ possibilities, whereas BruSLe is constrained to a reduced search space of $\binom{H \times W}{N}$, where the image size is $H \times W$ and BruSLe’s attack sparsity is $\frac{N}{H \times W}$. For positive integers N , H , and W , the following inequality always holds:

$$2^{3 \times H \times W} > \binom{H \times W}{N}. \quad (9)$$

This significant difference highlights GreedyPixel’s capacity to achieve finer granularity in adversarial manipulations.

Moreover, the comparison of the convergence curves between the fine-grained “white-box,” “black-box,” and “random mapping” (i.e., without using any surrogate model and priority map) strategies shows that our proposed priority map, coupled with precise gradient information, further accelerates convergence. Even without the priority map, our greedy algorithm consistently outperforms other methods, yielding lower loss values.

3.5. Algorithm of GreedyPixel Attack

Throughout the iterations of the pixel-wise greedy algorithm (details provided in Section 3.4), GreedyPixel processes pixels based on a priority map that dictates their order (details provided in Section 3.3). The algorithm terminates upon satisfying either of two stopping criteria:

- Maximum query reached: $t \times |E|^3 \leq Q$, where t and Q denote the current iteration and constrained maximum query number, respectively, and $0 \leq t \leq \frac{Q}{|E|^3}$;
- Success: $\ell < 0$, indicating a successful misclassification, where the prediction from the target model differs from the ground-truth label.

Therefore, t directly correlates with the number of queries made to the target model. Given the maximum query number Q , the query cost of GreedyPixel with these stop conditions is expressed as:

$$Q_{\text{Greedy}} = t \times |E|^3 \leq Q, \quad (10)$$

Algorithm 3 GreedyPixel Attack

Input: Original image x of size $C \times H \times W$ with $C = 3$, x 's ground-truth label y , target model Z , surrogate model Z_s , maximum L_∞ -norm magnitude ϵ , maximum query cost Q , periodicity N of updating the priority map.

Output: AE x' .

```

1:  $\delta_0 = 0 \in \mathbb{R}^{H \times W \times C}$ ,  $t = 0$  ▷ initialization
2: for  $t$  do
3:   if  $8 \times t > Q$  then
4:     Break
5:   end if
6:    $n = t \% N$  ▷ index in the priority map
7:   if  $n == 0$  then
8:      $\{(h_i, w_i)\}_{i=1}^{H \times W} = \text{Alg. 1}(x, y, Z_s)$ 
9:     ▷ priority map
10:  end if
11:   $\delta_{t+1}, \ell_{t+1} = \text{Alg. 2}(x, y, Z, \epsilon, (h_n, w_n), \delta_t)$ 
12:  ▷ greedy strategy
13:   $x' = x + \delta_{t+1}$ 
14:  if  $\ell_{t+1} < 0$  then
15:    Break
16:  end if
17: end for
18: return  $x'$ 

```

where $|E|$ denotes the number of options ($\{-\epsilon, +\epsilon\}$) available per channel. Equation (10) illustrates the efficiency of GreedyPixel relative to a brute-force approach (as detailed in Equation (4)), establishing it as a computationally practical method for generating AEs under resource constraints. The complete algorithm for the proposed GreedyPixel attack is outlined in Algorithm 3.

The variable t represents the number of pixel processing iterations, where some pixels may undergo processing multiple times. Therefore, t does not necessarily reflect the exact number of pixels that have been altered. When $t \geq H \times W$, it signifies that every pixel in the image has been processed at least once during the iterations. Consequently, the actual number of manipulated pixels is given by $\min(t, H \times W)$. This metric offers a more precise insight into the extent of GreedyPixel's impact on the image during the optimization process. Moreover, it highlights the relationship between the number of manipulated pixels and the query cost, both of which scale with the image dimensions $H \times W$. Thus, higher-resolution images inherently incur greater query costs.

4. Experiments

4.1. Datasets, Target, and Surrogate Models

We evaluated attacks using two sets of examples from two source datasets: CIFAR-10 [24] (sized to 32×32) and ImageNet [1] from the NIPS 2017 competition (cropped to 64×64 and 224×224 for ablation studies and to match the requirement of the target and surrogate models). Each set contains 1,000 examples.

We targeted models with varying architectures and layer sizes, as detailed in Table 3. Specifically, we evaluated the attack performance on four non-robust pretrained models: WideResNet-28-10 [10] for CIFAR-10

TABLE 3. MODEL ARCHITECTURES.

Dataset	Architecture	Role	Adversarial Training?
CIFAR-10	WideResNet-28-10 [10]	Target	NO
	WideResNet-28-10 [60]	Target	YES
	WideResNet-82-8 [3]	Target	YES
	XCiT-S12 [12]	Target	YES
	PreActResNet-18 [63]	Surrogate	YES
	PreActResNet-18 [19]*	Surrogate	YES
	RaWideResNet-70-16 [45]*	Surrogate	YES
ImageNet	ResNet-50 [10]	Target	NO
	ViT-Base-Patch16 [64]	Target	NO
	VGG19-BN [53]	Target	NO
	ConvNeXt [54]	Surrogate	YES
	Swin [27]*	Surrogate	YES
	ResNet-18 [49]*	Surrogate	YES

*denotes the surrogate model was assessed for ablation studies only.

TABLE 4. ATTACK SETTINGS.

Threat Model	Attack	Max. Q	ϵ	Sparsity
White-Box (Limited ϵ)	APGD [11]	Unlimited	4/255	N/A
	AutoAttack [11]			
	GreedyPixel (Ours)			
Black-Box (Limited ϵ)	DeCoW [26]	20,000	4/255	N/A
	MCG [67]			
	GFCS [33]			
	SQBA [44]			
	GreedyPixel (Ours)			
Black-Box (Unlimited ϵ)	BruSLe [56]	20,000	Unlimited	1%/0.1%*
	GreedyPixel (Ours)			N/A

*The sparsity for attacking CIFAR-10 and ImageNet was set to 1% (10 pixels) and 0.1% (50 pixels), respectively.

and ResNet-50 [10], ViT-Base-Patch16 [64], and VGG19-BN [53] for ImageNet, and three robust models employed as adversarial defenses (*i.e.*, adversarial training): WideResNet-28-10 [60], WideResNet-82-8 [3], and XCiT-S12 [12].

Furthermore, we conducted ablation studies on a range of surrogate models [19], [27], [45], [49], [54], [63], representing diverse architectures and algorithms, as presented in Table 3. For comparisons with other attacks that also require a surrogate model, all attacks were conducted using the same surrogate model to ensure fairness. In black-box scenarios, the surrogate model differed from the target model, whereas in white-box settings, the surrogate and target models were identical. Notably, GreedyPixel utilized adversarially pretrained models as surrogate models, as this approach led to enhanced visual quality. Conversely, non-adversarial surrogate models were simulated using random sequences, representing randomly distributed adversarial noise.

4.2. Benchmarks and Experimental Settings

The proposed GreedyPixel method was benchmarked against leading adversarial attack techniques under the three threat models described in Section 3.1. The specific attacks were selected from various strategies in Table 1 and their settings for each model are summarized in Table 4.

White-box attacks with constrained L_∞ -norm distance (*i.e.*, limited ϵ): Under this threat model, we

compared the performance of GreedyPixel to state-of-the-art (SOTA) gradient-based white-box attacks, specifically AutoAttack [11] and APGD [11], with a uniform perturbation constraint of $\epsilon = 4/255$. Consistent with white-box settings, the number of queries was unrestricted in this evaluation.

Black-box attacks with constrained L_∞ -norm distance (i.e., limited ϵ): In this scenario, GreedyPixel was evaluated against several prominent black-box attack methods, including DeCoW [26], GFCS [33], MCG [67], and SQBA [44] under the same constraint of $\epsilon = 4/255$. The DeCoW attack employs a purely transferable strategy, utilizing only a surrogate model without requiring query feedback from the target model. In contrast, GFCS and SQBA leverage both query feedback and transfer-based knowledge from a surrogate model. MCG, on the other hand, is a generator-based approach that solely relies on query feedback to train the generator. In all cases, the maximum number of queries (denoted as Max. Q) was set to 20,000, ensuring that GreedyPixel was evaluated against diverse black-box attack strategies under equitable conditions.

Black-box attacks with unconstrained L_∞ -norm distance (i.e., unlimited ϵ): For this threat model, we compared GreedyPixel to the SOTA sparse attack, BruSLe [56], which has demonstrated superior ASRs compared to earlier methods, such as the One-Pixel attack [55], without a constraint on ϵ . The sparsity of BruSLe was fixed at 1% (10 pixels) and 0.1% (50 pixels) for CIFAR-10 and ImageNet, respectively, and both BruSLe and GreedyPixel operated under a maximum query limit of 20,000.

Against adversarial defenses: Furthermore, we conducted evaluations of these attacks against established adversarial defense mechanisms, including the SOTA adversarial purification method, DiffPure [43], three latest adversarial training (AT) defenses [3], [12], [60], and one adversarial detection [36], across all three threat models.

4.3. Evaluation Metrics

The evaluation metrics encompassed several key aspects to comprehensively assess the performance of the proposed attack and benchmark methods. ASR was employed to measure attack effectiveness, where a higher ASR indicates greater success in manipulating model predictions. To assess visual quality, we employed the Structural Similarity Index Measure (SSIM) [62] and Learned Perceptual Image Patch Similarity (LPIPS) [68], where higher SSIM and lower LPIPS values denote subtler deviations from the original images. These two perceptual metrics offer a quantitative evaluation of visual quality from complementary perspectives. Time cost measured the time efficiency of attack execution, with smaller durations indicating faster attack. Additionally, the average number of queries (denoted as Avg. Q) reflected query efficiency, where fewer queries signify more efficient utilization of resources. When evaluating attacks against defenses, in addition to the ASR, we introduced the adversarial detection rate as a complementary metric. This rate quantifies the proportion of AEs identified as threats by the adversarial detection mechanism. A lower detection rate indicates higher attack efficacy, as it reflects the ability of the AEs to evade detection. Together, these metrics provided

TABLE 5. ATTACK PERFORMANCE ON WIDERESNET-28-10 MODEL [10] AND CIFAR-10 DATASET [24].

Threat Model	Attack	Time(s)↓	Avg. Q↓	ASR(%)↑	LPIPS↓	SSIM↑
White-Box (Limited ϵ)	APGD	1.7		100	0.0006	0.981
	AutoAttack	1.7	Unlimited	100	0.0006	0.982
	Ours	1.3		100	0.0001	0.994
Black-Box (Limited ϵ)	DeCoW*	28	0	8.7	0.0022	0.986
	MCG	3.7	745	99.5	0.0013	0.978
	SQBA*	81	17,418	13.0	0.0016	0.988
	Ours	1.8	1,997	100	0.0002	0.995
Black-Box (Unlimited ϵ)	BruSLe	1.4	367	98.7	0.0168	0.876
	Ours	0.3	318	100	0.0023	0.964

*DeCoW [26] and SQBA [44] exhibit limited transferability when there is a significant discrepancy between the surrogate model (PreActResNet-18 [63]) and the target model (WideResNet-28-10 [10]). To ensure the correctness of our implementation, we evaluated their performance in a white-box attack setting (where the surrogate and target models are identical), achieving success rates of 70.5% and 84.3%, respectively.

Bold denotes superior performance.

a comprehensive evaluation framework that assessed the efficacy, computational efficiency, and perceptual quality of the adversarial attacks implemented in our experiments. The formal definitions of ASR, SSIM, LPIPS, and adversarial detection rate are provided in Appendix B.

4.4. Implementation

Our implementation utilized ART [42] and Robust-Bench [10], integrated with PyTorch. The experiments were conducted on a machine equipped with an NVIDIA A100 40-GB GPU.

5. Performance

5.1. Attack Efficacy

We evaluated the proposed GreedyPixel attack and benchmarked its performance against SOTA attacks across three distinct threat models (refer to Section 4.2). Attack efficacy is measured in terms of ASR. As summarized in Tables 5 to 8, GreedyPixel consistently achieved higher ASRs compared to other methods under the same conditions. However, white-box GreedyPixel attacks demonstrated superior performance relative to their black-box counterparts, which are constrained by a limited number of queries. Moreover, GreedyPixel exhibited greater efficacy on low-resolution datasets (such as CIFAR-10) compared to high-resolution datasets (such as ImageNet) under black-box conditions, likely due to the fact that, within a restricted query budget, only a subset of pixels can be modified, which may be insufficient to ensure successful attacks.

5.2. Attack Efficiency

We assessed the efficiency of the proposed GreedyPixel attack from two key perspectives: time cost and query efficiency. As illustrated in Tables 5 to 8, GreedyPixel outperforms all black-box attacks in terms of time efficiency, positioning it as the most rapid approach among its competitors. Although GreedyPixel requires a greater

TABLE 6. ATTACK PERFORMANCE ON RESNET-50 MODEL [10] AND IMAGENET DATASET [1].

Threat Model	Attack	Time(s)↓	Avg. Q↓	ASR(%)↑	LPIPS↓	SSIM↑
White-Box (Limited ϵ)	APGD	2.5		99.9	0.0351	0.954
	AutoAttack	2.6	Unlimited	100	0.0343	0.955
	Ours	23		100	0.0006	0.997
Black-Box (Limited ϵ)	DeCoW*	536	0	8.0	0.0356	0.944
	GFCS	259	12,217	42.2	0.0229	0.978
	SQBA*	101	15,538	21.6	0.0224	0.971
	Ours	26	13,152	60.0	0.0002	≈ 1
Black-Box (Unlimited ϵ)	BruSLe	7.2	913	98.0	0.0616	0.977
	Ours	2	980	99.9	0.0232	0.985

*DeCoW [26] and SQBA [44] exhibit limited transferability when there is a significant discrepancy between the surrogate model (ConvNeXt [54]) and the target model (ResNet-50 [10]). To ensure the correctness of our implementation, we evaluated their performance in a white-box attack setting (where the surrogate and target models are identical), achieving success rates of 94.9% and 99.6%, respectively.

Bold denotes superior performance.

TABLE 7. ATTACK PERFORMANCE ON ViT-BASE-PATCH16 MODEL [64] AND IMAGENET DATASET [1].

Threat Model	Attack	Time(s)↓	Avg. Q↓	ASR(%)↑	LPIPS↓	SSIM↑
White-Box (Limited ϵ)	APGD	2.6		100	0.0349	0.958
	AutoAttack	2.6	Unlimited	100	0.0333	0.959
	Ours	63		100	0.0013	0.995
Black-Box (Limited ϵ)	DeCoW*	536	0	3.8	0.0356	0.944
	GFCS	347	15,769	24.0	0.0239	0.978
	SQBA*	112	18,024	9.6	0.0240	0.951
	Ours	65	16,096	37.8	0.0004	0.999
Black-Box (Unlimited ϵ)	BruSLe	10	1,509	98.6	0.0641	0.977
	Ours	6.6	1,620	100	0.0341	0.978

*DeCoW [26] and SQBA [44] exhibit limited transferability when there is a significant discrepancy between the surrogate model (ConvNeXt [54]) and the target model (ViT-Base-Patch16 [64]). To ensure the correctness of our implementation, we evaluated their performance in a white-box attack setting (where the surrogate and target models are identical), achieving success rates of 78% and 83.1%, respectively.

Bold denotes superior performance.

number of queries compared to other query-based attacks, such as DeCoW [26], GFCS [33], and MCG [67], it compensates for this by delivering superior outcomes in terms of ASRs, time cost, and visual quality (higher SSIM and lower LPIPS scores). The improved time efficiency, despite the higher query demand, is attributed to GreedyPixel’s ability to compute eight queries in parallel ($|E|^3 = 8$, as discussed in Section 3.4), whereas other attacks execute queries sequentially. Moreover, in scenarios where the L_∞ -norm constraint (ϵ) is relaxed, GreedyPixel demonstrates either comparable or superior attack efficiency when benchmarked against the SOTA sparse attack, BruSLe [56].

However, the complexity of attacking high-resolution images (e.g., ImageNet) increases more sharply for GreedyPixel compared to low-resolution images (e.g., CIFAR-10). Despite this, GreedyPixel achieves a 100% ASR for white-box attacks on CIFAR-10, doing so more rapidly than prominent methods such as APGD [11] and AutoAttack [11]. In contrast, when applied to ImageNet, although it remains highly effective, GreedyPixel is less time-efficient than APGD and AutoAttack, highlighting the trade-off between resolution

TABLE 8. ATTACK PERFORMANCE ON VGG19-BN MODEL [53] AND IMAGENET DATASET [1].

Threat Model	Attack	Time(s)↓	Avg. Q↓	ASR(%)↑	LPIPS↓	SSIM↑
White-Box (Limited ϵ)	APGD	0.8		100	0.0254	0.964
	AutoAttack	0.9	Unlimited	100	0.0246	0.965
	Ours	26		100	0.0012	0.996
Black-Box (Limited ϵ)	DeCoW*	536	0	36.6	0.0356	0.944
	GFCS	125	6,198	71.5	0.0124	0.984
	SQBA*	39	9,846	50.1	0.0162	0.978
	Ours	13	6,662	84.7	0.0001	≈ 1
Black-Box (Unlimited ϵ)	BruSLe	1.9	391	99.3	0.0580	0.978
	Ours	1	477	99.9	0.0111	0.993

*DeCoW [26] and SQBA [44] exhibit limited transferability when there is a significant discrepancy between the surrogate model (ConvNeXt [54]) and the target model (VGG19-BN [53]). To ensure the correctness of our implementation, we evaluated their performance in a white-box attack setting (where the surrogate and target models are identical), achieving success rates of 99.2% and 99.9%, respectively.

Bold denotes superior performance.

and computational cost.

5.3. Visual Quality

We computed the SSIM and LPIPS scores between the original inputs and AEs to assess the visibility of adversarial perturbations. Additionally, we visualized these perturbations to compare the qualitative differences among algorithms, which result in varying visual quality. The grayscale perturbation illustration δ_{Gray} in Figure 4 was generated through a two-step process. First, the actual perturbations δ were normalized from the range $[\epsilon_{min}, \epsilon_{max}]$ to $[0, 1]$ to produce δ_{RGB} . Subsequently, δ_{RGB} was converted to grayscale using the NTSC formula [31]:

$$\delta_{RGB} = \frac{\delta - \epsilon_{min}}{\epsilon_{max} - \epsilon_{min}}, \quad (11)$$

$$\delta_{Gray} = 0.299 \cdot \delta_{RGB} \cdot R + 0.587 \cdot \delta_{RGB} \cdot G + 0.114 \cdot \delta_{RGB} \cdot B,$$

where $\delta_{RGB} \cdot R$, $\delta_{RGB} \cdot G$, and $\delta_{RGB} \cdot B$ represent the red, green, and blue channels, respectively.

As presented in Tables 5 to 8, the GreedyPixel attack consistently outperforms all leading adversarial methods in terms of visual quality, as evidenced by higher SSIM and lower LPIPS scores. This is further illustrated in Figure 4, where our method introduces less noticeable noise, particularly in black-box settings. GreedyPixel, being a pixel-wise algorithm similar to the BruSLe attack [56], modifies fewer pixels compared to methods like AutoAttack [11], DeCoW [26], GFCS [33], MCG [67], and SQBA [44], resulting in more subtle and visually imperceptible changes. More critically, our approach effectively targets robust features within the image, concentrating perturbations around complex objects and edges rather than indiscriminately affecting background regions, as observed with BruSLe. This targeted manipulation enables GreedyPixel to achieve the highest visual quality across all attack mechanisms, underscoring its superiority in generating minimally invasive yet highly effective adversarial perturbations.

	Original	White-Box (Limited ϵ)		Black-Box (Limited ϵ)				Black-Box (Unlimited ϵ)	
		AutoAttack	Ours	MCG	SQBA	DeCoW	Ours	BruSLe	Ours
CIFAR-10									
	LPIPS↓	0.0006	0.0001	0.0013	0.0162	0.0022	0.0002	0.0168	0.0023
	SSIM↑	0.982	0.994	0.978	0.988	0.986	0.995	0.876	0.964
	ASR (%)↑	100	100	99.5	13.0	8.7	100	98.7	100
ImageNet									
	LPIPS↓	0.0343	0.0006	0.0229	0.0224	0.0356	0.0002	0.0616	0.0232
	SSIM↑	0.955	0.997	0.978	0.971	0.944	0.9995	0.977	0.985
	ASR (%)↑	100	100	42.2	21.6	8.0	60.0	98.0	99.9

Figure 4. Comparison of AEs generated by different attack algorithms in terms of visual quality and perturbation appearance. The proposed GreedyPixel method achieves the highest visual quality by selectively modifying only critical pixels. The perturbations are re-scaled for visual inspection using Equation (11), with **bold** indicating superior performance. Notably, while the BruSLe attack [56] introduces fewer perturbed pixels compared to GreedyPixel, the visibility of these perturbations is higher due to their positional placement.

TABLE 9. USER STUDY RESULTS FOR VISUAL QUALITY OF AEs: INVISIBLE RATE REPRESENTS THE PERCENTAGE OF EXAMPLES WITH IMPERCEPTIBLE PERTURBATIONS, INDICATING SUPERIOR VISUAL QUALITY.

Threat Model	Attack	CIFAR-10		ImageNet	
		ASR (%) ↑	Invisible Rate ↑	ASR (%) ↑	Invisible Rate ↑
White-Box (Limited ϵ)	AutoAttack	100	27/50	100	32/50
	GreedyPixel (ours)	100	43/50	100	49/50
Black-Box (Limited ϵ)	MCG	99.5	6/50	-	-
	GFCS	-	-	42.2	42/50
	GreedyPixel (ours)	100	47/50	60.0	49/50
Black-Box (Unlimited ϵ)	BruSLe	98.7	0/50	98.0	3/50
	GreedyPixel (ours)	100	2/50	99.9	18/50

MCG and GFCS did not release their code for ImageNet and CIFAR-10 datasets, respectively.

Bold denotes superior performance.

5.4. User Study on Visual Quality

We conducted user studies to evaluate the human perceptual visual quality of AEs. Specifically, we randomly selected 50 original images, which were successfully attacked by all six distinct attack methods, including the white-box AutoAttack [11], black-box GFCS [33] and MCG [67] attacks, the sparse BruSLe attack [56], and our GreedyPixel under three threat models, as outlined in Table 4. These attacks were applied to two datasets—CIFAR-10, comprising low-resolution images, and ImageNet, consisting of high-resolution images. For each dataset, we designed a 50-question questionnaire, as illustrated in Figure 9 of Appendix A. Ten participants (the

number chosen based on the 10 ± 2 rule [23]) with varying levels of vision, including individuals with and without corrective lenses, were asked to identify AEs that they perceived as visually indistinguishable from the original images. The test samples were presented in a randomized order to minimize bias towards specific attack methods. APGD [11] and DeCoW [26] were excluded from the user study. APGD was omitted due to its perturbation patterns closely resembling those of AutoAttack, while DeCoW was excluded due to its significantly lower ASRs.

The user study results, as shown in Table 9, demonstrate that the proposed GreedyPixel attack achieves markedly superior visual quality, with a greater number of AEs that were difficult for participants to distinguish

TABLE 10. ATTACK PERFORMANCE (%) AGAINST ADVERSARIAL DEFENSES DURING COUNTERATTACK EXPERIMENTS.

Threat Model	Attack	No Defense	Purification ^a [43] ↑	AT [60] ↑	AT [3] ↑	AT [12] ↑	Detection ^b [36] ↓
White-Box (Limited ϵ)	APGD	100	20.5	16.0	13.1	20.7	10.7
	AutoAttack	100	21.5	16.7	14.2	21.8	10.6
	GreedyPixel (ours)	100	25.4	16.5	14.0	21.4	8.4
Black-Box (Limited ϵ)	DeCoW ^c	8.7	16.2	9.9	9.0	13.4	7.7
	MCG	99.5	13.2	15.3	13.3	20	7.9
	SQBA	13.0	17.5	10.3	9.3	15.1	8.2
	GreedyPixel (ours)	100	23.4	16.4	14.0	21.3	8.5
Black-Box (Unlimited ϵ)	BruSLe	98.7	30.8	72.5	75.5	57.1	81.9
	GreedyPixel (ours)	100	36.2	84.6	82.7	93.2	31.5

^aDiffusion timestep=0.1.

^bThe detector is trained with knowledge of Adversarial Patch [5], DeepFool [39], FGSM [18], PGD [35], APGD [11], Spatial Transformation [66], and Square [2] attacks. The threshold is set for a 5% clean rejection rate.

^cDeCoW [26] demonstrates suboptimal performance when utilizing the surrogate model [63], irrespective of whether it targets non-robust or robust models. The increase in ASR against DiffPure is likely attributable to the distortion dominating over adversarial manipulations.

Bold denotes superior performance.



ϵ	4/255	8/255	16/255	32/255	64/255	128/255	255/255
LPIPS↓	0.0002	0.0007	0.0019	0.0041	0.0091	0.0182	0.0232
SSIM↑	0.9995	0.999	0.997	0.994	0.990	0.986	0.986
Avg. Q↓	13152	8772	5040	2793	1656	1123	980
Time Cost (s)↓	26	18	11	5.7	3.4	2.3	2
ASR (%)↑	60.0	85.8	97.5	99.5	99.8	99.9	99.9

Figure 5. Visual quality, efficiency, and ASRs under different L_∞ -norm attack budgets. The proposed GreedyPixel allows for higher attack budgets, trading slight visual quality degradation (see SSIM and LPIPS) for improved efficiency and ASRs.

from the original images, particularly in both white-box and black-box settings under limited ϵ . Under conditions of unlimited ϵ , both the BruSLe and GreedyPixel attacks were more easily detected, though our method continued to exhibit better performance. Furthermore, when comparing the results from CIFAR-10 and ImageNet, it was observed that perturbations on low-resolution images (CIFAR-10) were more readily identifiable than those on high-resolution images (ImageNet), suggesting that high-resolution images present a greater challenge for defense mechanisms.

5.5. Counterattack on Adversarial Defenses

We conducted counterattacks against three adversarial training (AT) methods [3], [12], [60], an adversarial purification method (DiffPure [43]), and an adversarial detector [36], utilizing the CIFAR-10 dataset. The AEs were fully trained over 20,000 queries without early stopping, applied in both white-box and black-box scenarios. We posit that targeting systems that incorporate defenses is a more pragmatic assumption in real-world applications, given the rapid advancements in adversarial defense technologies.

The results, as outlined in Table 10, indicate that our proposed GreedyPixel method is notably more effective against adversarial defenses, achieving comparable or higher ASRs, and comparable or lower adversarial detection rates than other leading methods across all three threat models. This highlights the enhanced aggressiveness and

adaptability of GreedyPixel in circumventing adversarial defenses.

6. Ablation Study

6.1. Attack Constraint

We investigated the impact of increasing attack budgets. The visual quality comparisons in Figure 4 demonstrate that under a small L_∞ -norm constraint of 4/255, our method significantly outperforms other attacks in terms of SSIM and LPIPS scores. This suggests that increasing the attack budget may maintain visual quality superior to that of other attacks, while enhancing ASRs and attack efficiency. The results presented in Figure 5 support our hypothesis that our attack method can trade slight visual quality degradation (see SSIM and LPIPS) for improved attack efficiency and higher ASRs.

6.2. Periodicity of Updating the Priority Map

We strategically design the update frequency of the priority map to further enhance the visual quality of AEs as measured by LPIPS and SSIM, while acknowledging a trade-off in the ASR. By updating the priority map and resetting the adversary sequence from the most crucial pixel identified in the updated map, the adversary is directed to focus on more critical pixels. As shown in

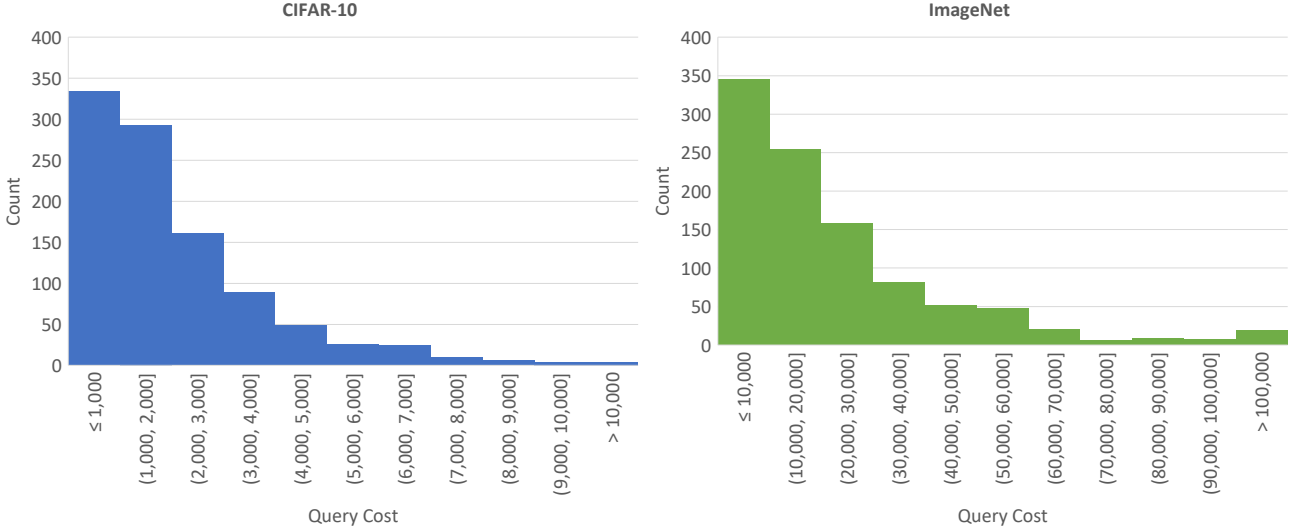


Figure 6. Query costs and distribution of successful AEs. This figure illustrates the distribution of query costs among successful AEs, demonstrating that the majority of these examples require relatively few queries to succeed. While increasing the allowed number of queries can improve attack performance, the rate of improvement diminishes as the query limit grows larger. Beyond a certain point (10,000 queries / 1,250 pixels for CIFAR-10, or 100,000 queries / 12,500 pixels for ImageNet), further increases mainly affect the few remaining unsuccessful cases, leading to marginal gains in overall performance.

TABLE 11. THE PERFORMANCE OF UPDATING THE PRIORITY MAP IN VARIOUS PERIOD. THE TARGET MODEL AND DATASET ARE WIDERESNET-28-10 [10] AND CIFAR-10 [24], RESPECTIVELY.

Threat Model	Sparsity	Update Period	ASR (%) \uparrow	LPIPS \downarrow	SSIM \uparrow
White-Box (Limited ϵ)	10%	Disable	50.3	≈ 0	0.997
	30%	Disable	90.3	≈ 0	0.995
	50%	Disable	98.6	0.0001	0.994
	Disable	$N = 100$	97.4	≈ 0	0.995
	Disable	$N = 300$	99.7	≈ 0	0.994
	Disable	$N = 500$	100	0.0001	0.994
	Disable	Disable	100	0.0001	0.994
Black-Box (Limited ϵ)	10%	Disable	29.9	≈ 0	0.998
	30%	Disable	86.1	0.0001	0.997
	50%	Disable	97.6	0.0002	0.996
	Disable	$N = 100$	40.0	≈ 0	0.998
	Disable	$N = 300$	91.6	0.0001	0.996
	Disable	$N = 500$	98.8	0.0002	0.996
	Disable	Disable	100	0.0002	0.995

Bold denotes superior performance.

Table 11, increasing the update frequency of the priority map (*i.e.*, reducing N in Algorithm 3) leads to improved LPIPS and SSIM scores, indicating better visual quality, albeit at the cost of a reduced ASR.

Furthermore, we explored an alternative strategy where sparsity is fixed by generating the priority map only once but resetting the adversary sequence every N iterations (*i.e.*, every N pixels). As demonstrated in Table 11, decreasing sparsity also enhances visual quality but results in a more pronounced drop in ASR. Due to its comparatively lower practicality than the proposed algorithm, we opted not to highlight this alternative.

6.3. Maximum Queries Limit

In query-based adversarial attacks, the maximum query limit plays a pivotal role in determining attack efficacy, particularly when dealing with challenging images.

This limit is inherently linked to the number of manipulable pixels, as outlined in Equation (10). Our analysis, presented in Table 12, highlights the effects of varying the query limit across multiple performance metrics. For instance, setting a very low query threshold (*e.g.*, 5,000 queries for CIFAR-10, equating to 625 pixels out of 1,024, or 20,000 queries for ImageNet, affecting 2,500 pixels out of 50,176) hampers ASRs, as it restricts the number of pixels that can be altered. However, increasing the threshold beyond 10,000 queries (1,250 pixels for CIFAR-10) or 100,000 queries (12,500 pixels for ImageNet) results in minimal further improvements in efficacy. In these higher-query settings, average query counts (Avg. Q), time costs, and perceptual metrics such as LPIPS and SSIM exhibit little variation. This plateau effect arises because the increased query allowance predominantly impacts a small number of previously unsuccessful cases, as shown by the high-query-cost instances in Figure 6, where insufficient queries had been the limiting factor. Additionally, the ASRs under higher-query settings demonstrate that, given sufficient time and query resources, our GreedyPixel attack can achieve solutions comparable to those of gradient-based algorithms, without requiring access to gradient information, aligning with our theoretical analysis in Section 3.4.

6.4. Image Resolution

As shown in Table 12, under an unconstrained query setting, the ASRs approach 100% as image resolution increases, achieving results comparable to those on low-resolution images, albeit with a higher computational cost. However, under a constrained query budget, higher image resolution imposes a trade-off, resulting in reduced ASRs for high-resolution images. This highlights the increased difficulty faced by GreedyPixel in effectively attacking high-resolution images.

TABLE 12. BLACK-BOX ATTACK PERFORMANCE EVALUATION WITH A FIXED PERTURBATION LIMIT OF $\epsilon = 4/255$, UNDER VARYING MAXIMUM QUERY CONSTRAINTS.

Resolution	Max. Q	Avg. Q	Time (s)	ASR (%)	LPIPS	SSIM
32×32 (CIFAR-10)	5K	1,863	1.7	92.6	0.0002	0.996
	10K	1,993	1.8	99.6	0.0002	0.995
	15K	1,997	1.8	100	0.0002	0.995
	20K	1,997	1.8	100	0.0002	0.995
64×64 (ImageNet)	10K	2,687	4.7	94.9	0.0003	0.999
	20K	2,957	5.1	98.8	0.0003	0.999
	50K	3,108	5.5	99.7	0.0003	0.998
	100K	3,259	5.5	100	0.0003	0.998
224×224 (ImageNet)	20K	13,152	26	60.0	0.0002	≈ 1
	50K	19,598	40	89.2	0.0004	0.999
	100K	21,816	44	98.1	0.0005	0.999
	200K	22,617	47	99.6	0.0005	0.999
	400K	23,003	47	99.9	0.0005	0.999

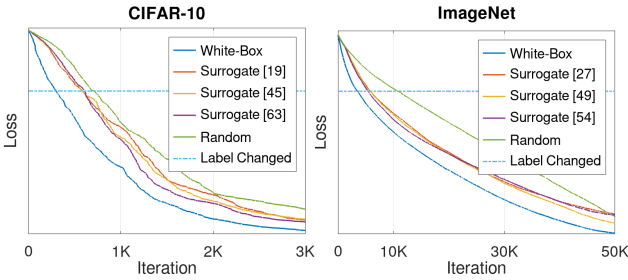


Figure 7. The proposed pixel-wise priority map effectively reduces the number of queries, with potential for further enhancement when incorporating white-box knowledge.

6.5. Priority Map with Different Surrogate Models

We investigated the impact of using a priority map, which was learned using different surrogate models. The selected surrogate models included RaWideResNet-70-16 [45] and two types of PreActResNet-18 [19], [63] for CIFAR-10, and ConvNeXt [54], Swin [27], and ResNet-18 [49] for ImageNet, each representing diverse architectures and levels of robustness.

The results presented in Table 13 reveal several key insights. First, the incorporation of the priority map significantly enhances attack efficiency, as evidenced by reductions in both average query count and time cost, when compared to the “Random” approach, which lacks this prioritization mechanism. This improvement is particularly pronounced in scenarios where query numbers are constrained, such as when attacking high-resolution images (*e.g.*, ImageNet), leading to higher ASRs. Second, the integration of “white-box” knowledge further amplifies both the efficacy and efficiency of the attack, owing to the reduction in attack cost facilitated by the precise gradient information. Lastly, employing adversarially trained models as surrogate models improves the visual quality of the AEs compared to non-robust models (see “white-box” results) and random approaches, though this improvement is less pronounced.

These observations are corroborated by the data in Figure 7. The priority map expedites convergence, reducing the number of queries necessary to achieve comparable loss values relative to the “Random” approach. Further-



Figure 8. Model-inversion attack generations from the same source image to the same target image. Square [2] and BruSLe [56] attacks introduce significant differences.

more, the incorporation of “white-box” knowledge enhances efficiency, as reflected in the superior performance of the “White-box” curves. Collectively, these results underscore the importance of our strategy, particularly when attacking high-resolution images where query efficiency is a critical limiting factor.

7. Discussion

7.1. Alternative Strategies

We have demonstrated that the order of processing pixels is crucial for efficiency. Here, we briefly discuss alternative strategies apart from the proposed pixel-wise priority map. First, one might consider increasing the number of queries until the attack succeeds. However, this approach is impractical due to high time costs, potential query blocking, and degradation of visual quality from increased manipulations. Second, alternatives like region-, objective-, edge-, or attention-based maps introduce multiple pixels with the same priority, requiring processing all pixels within the same group, which is less efficient. Therefore, we are confident that our algorithm is optimal based on current knowledge.

7.2. Manipulation on Sensitive Entities

Our recent work emphasizes the critical importance of fine-grained manipulations, like our GreedyPixel attack, particularly when targeting sensitive entities such as the latent codes in diffusion models. In contrast, other black-box methods, including Square [2] and BruSLe [56] attacks, often produce noticeable distortions or noise during the generation process, as illustrated in Figure 8.

8. Conclusion & Future Research

In this paper, we present GreedyPixel, a novel pixel-wise strategy for black-box adversarial attacks. GreedyPixel optimizes pixel manipulation sequences using a priority map, achieving high ASRs while minimizing pixel changes, and is particularly effective for smaller images. Overall, GreedyPixel represents a significant advancement in adversarial attack methodologies, enhancing efficacy and visual quality in probing machine learning model vulnerabilities.

Future research will focus on refining the priority map and exploring applications across diverse datasets and defenses. For example, GreedyPixel can be adapted into a sparse attack similar to BruSLe [26] and One-Pixel [55] attacks by periodically updating the priority map, concentrating adjustments primarily on a limited set

TABLE 13. ATTACK PERFORMANCE EVALUATION WITH A FIXED PERTURBATION LIMIT OF $\epsilon = 4/255$ AND MAXIMUM QUERY CONSTRAINT OF 20,000 (INCLUDING WHITE-BOX ATTACKS), UNDER VARYING SURROGATE MODELS.

Dataset	Target	Surrogate	Avg. Q ↓	Time Cost (s) ↓	ASR (%) ↑	LPIPS ↓	SSIM ↑
CIFAR-10	WideResNet-28-10 [10]	WideResNet-28-10 [10] ^a	1,510	1.3	100	0.0001	0.994
		PreActResNet-18 [63]	1,997	1.8	100	0.0002	0.995
		PreActResNet-18 [19]	2,052	1.8	100	0.0002	0.995
		RaWideResNet-70-16 [45]	2,040	1.8	100	0.0002	0.995
		Random ^b	2,220	2.1	100	0.0001	0.994
ImageNet	ResNet-50 [10]	ResNet-50 [10] ^a	7,826	16	86.1	0.0005	0.997
		ConvNeXt [54]	13,152	26	60.0	0.0002	0.9995
		Swin [27]	13,242	27	59.2	0.0003	0.999
		ResNet-18 [49]	13,563	27	57.6	0.0002	0.999
		Random ^b	14,149	27	54.9	0.0004	0.997

^aRefers to white-box attacks, where the surrogate model is identical to the target model.

^bDenotes the use of a random map, with no priority calculation for pixel selection.

of high-priority pixels. One limitation is that the query numbers increase rapidly with the image size, which we aim to address in our future work as well.

References

- [1] Ian Goodfellow Alex K, Ben Hamner. Nips 2017: Defense against adversarial attack, 2017.
- [2] Maksym Andriushchenko, Francesco Croce, Nicolas Flammarion, and Matthias Hein. Square attack: a query-efficient black-box adversarial attack via random search. In *European Conference on Computer Vision (ECCV)*, pages 484–501, 2020.
- [3] Brian R Bartoldson, James Diffenderfer, Konstantinos Parasyris, and Bhavya Kaikhura. Adversarial robustness limits via scaling-law and human-alignment studies. In *2nd Workshop on Advancing Neural Network Training: Computational Efficiency, Scalability, and Resource Optimization (WANT @ ICML 2024)*, 2024.
- [4] Yoshua Bengio, Patrice Simard, and Paolo Frasconi. Learning long-term dependencies with gradient descent is difficult. *IEEE Transactions on Neural Networks*, 5(2):157–166, 1994.
- [5] Tom B Brown, Dandelion Mané, Aurko Roy, Martín Abadi, and Justin Gilmer. Adversarial patch. *arXiv preprint arXiv:1712.09665*, 2017.
- [6] Zikui Cai, Chengyu Song, Srikanth Krishnamurthy, Amit Roy-Chowdhury, and Salman Asif. Blackbox attacks via surrogate ensemble search. *Advances in Neural Information Processing Systems (NeurIPS)*, 35:5348–5362, 2022.
- [7] Han Cao, Qindong Sun, Yaqi Li, Rong Geng, and Xiaoxiong Wang. Efficient history-driven adversarial perturbation distribution learning in low frequency domain. *ACM Transactions on Privacy and Security*, 27(1):1–25, 2024.
- [8] Nicholas Carlini and David Wagner. Towards evaluating the robustness of neural networks. In *2017 IEEE Symposium on Security and Privacy (S&P)*, pages 39–57, 2017.
- [9] Gilad Cohen, Guillermo Sapiro, and Raja Giryes. Detecting adversarial samples using influence functions and nearest neighbors. In *Proceedings of the IEEE/CVF Conference on Computer Vision and Pattern Recognition (CVPR)*, pages 14453–14462, 2020.
- [10] Francesco Croce, Maksym Andriushchenko, Vikash Sehwal, Edoardo Debenedetti, Nicolas Flammarion, Mung Chiang, Prateek Mittal, and Matthias Hein. Robustbench: a standardized adversarial robustness benchmark. In *Thirty-fifth Conference on Neural Information Processing Systems Datasets and Benchmarks Track (Round 2) (NeurIPS 2021)*, 2021.
- [11] Francesco Croce and Matthias Hein. Reliable evaluation of adversarial robustness with an ensemble of diverse parameter-free attacks. In *International Conference on Machine Learning (ICML)*, pages 2206–2216, 2020.
- [12] Edoardo Debenedetti, Vikash Sehwal, and Prateek Mittal. A light recipe to train robust vision transformers. In *2023 IEEE Conference on Secure and Trustworthy Machine Learning (SaTML)*, pages 225–253, 2023.
- [13] Jiankang Deng, Jia Guo, Niannan Xue, and Stefanos Zafeiriou. Arcface: Additive angular margin loss for deep face recognition. In *Proceedings of the IEEE/CVF Conference on Computer Vision and Pattern Recognition (CVPR)*, pages 4690–4699, 2019.
- [14] Junhao Dong, Seyed-Mohsen Moosavi-Dezfooli, Jianhuang Lai, and Xiaohua Xie. The enemy of my enemy is my friend: Exploring inverse adversaries for improving adversarial training. In *Proceedings of the IEEE/CVF Conference on Computer Vision and Pattern Recognition (CVPR)*, pages 24678–24687, 2023.
- [15] Xiaoyi Dong, Dongdong Chen, Jianmin Bao, Chuan Qin, Lu Yuan, Weiming Zhang, Nenghai Yu, and Dong Chen. Greedyfool: Distortion-aware sparse adversarial attack. *Advances in Neural Information Processing Systems (NeurIPS)*, 33:11226–11236, 2020.
- [16] Yan Feng, Baoyuan Wu, Yanbo Fan, Li Liu, Zhifeng Li, and Shu-Tao Xia. Boosting black-box attack with partially transferred conditional adversarial distribution. In *Proceedings of the IEEE/CVF Conference on Computer Vision and Pattern Recognition (CVPR)*, pages 15095–15104, 2022.
- [17] Iuri Frosio and Jan Kautz. The best defense is a good offense: Adversarial augmentation against adversarial attacks. In *Proceedings of the IEEE/CVF Conference on Computer Vision and Pattern Recognition (CVPR)*, pages 4067–4076, 2023.
- [18] Ian J Goodfellow, Jonathon Shlens, and Christian Szegedy. Explaining and harnessing adversarial examples. *arXiv preprint arXiv:1412.6572*, 2014.
- [19] Sven Gowal, Sylvestre-Alvise Rebuffi, Olivia Wiles, Florian Stimberg, Dan Andrei Calian, and Timothy A Mann. Improving robustness using generated data. *Advances in Neural Information Processing Systems (NeurIPS)*, 34:4218–4233, 2021.
- [20] Chuan Guo, Mayank Rana, Moustapha Cisse, and Laurens van der Maaten. Countering adversarial images using input transformations. In *International Conference on Learning Representations (ICLR)*, 2018.
- [21] Thomas Hickling, Nabil Aouf, and Philippa Spencer. Robust adversarial attacks detection based on explainable deep reinforcement learning for uav guidance and planning. *IEEE Transactions on Intelligent Vehicles*, 2023.
- [22] Geoffrey E Hinton, Simon Osindero, and Yee-Whye Teh. A fast learning algorithm for deep belief nets. *Neural Computation*, 18(7):1527–1554, 2006.
- [23] Wonil Hwang and Gavriel Salvendy. Number of people required for usability evaluation: the 10±2 rule. *Communications of the ACM*, 53(5):130–133, 2010.
- [24] Alex Krizhevsky, Geoffrey Hinton, et al. Learning multiple layers of features from tiny images. Technical report, University of Toronto, 2009.
- [25] Bin Liang, Hongcheng Li, Miaoqiang Su, Xirong Li, Wenchang Shi, and Xiaofeng Wang. Detecting adversarial image examples in deep neural networks with adaptive noise reduction. *IEEE Transactions on Dependable and Secure Computing*, 18(1):72–85, 2021.

- [26] Qinliang Lin, Cheng Luo, Zenghao Niu, Xilin He, Weicheng Xie, Yuanbo Hou, Linlin Shen, and Siyang Song. Boosting adversarial transferability across model genus by deformation-constrained warping. In *Proceedings of the AAAI Conference on Artificial Intelligence (AAAI)*, pages 3459–3467, 2024.
- [27] Chang Liu, Yinpeng Dong, Wenzhao Xiang, Xiao Yang, Hang Su, Jun Zhu, Yuefeng Chen, Yuan He, Hui Xue, and Shibao Zheng. A comprehensive study on robustness of image classification models: Benchmarking and rethinking. *arXiv preprint arXiv:2302.14301*, 2023.
- [28] Jun Liu, Jiantao Zhou, Jiandian Zeng, and Jinyu Tian. Difattack: Query-efficient black-box adversarial attack via disentangled feature space. In *Proceedings of the AAAI Conference on Artificial Intelligence (AAAI)*, pages 3666–3674, 2024.
- [29] Renyang Liu, Wei Zhou, Tianwei Zhang, Kangjie Chen, Jun Zhao, and Kwok-Yan Lam. Boosting black-box attack to deep neural networks with conditional diffusion models. *IEEE Transactions on Information Forensics and Security*, 19:5207–5219, 2024.
- [30] Xiaoxuan Liu, Livia Faes, Aditya U Kale, Siegfried K Wagner, Dun Jack Fu, Alice Bruynseels, Thushika Mahendiran, Gabriella Moraes, Mohith Shandas, Christoph Kern, et al. A comparison of deep learning performance against health-care professionals in detecting diseases from medical imaging: a systematic review and meta-analysis. *The lancet digital health*, 1(6):e271–e297, 2019.
- [31] DC Livingston. Colorimetric analysis of the ntsc color television system. *Proceedings of the IRE*, 42(1):138–150, 1954.
- [32] Yuyang Long, Qilong Zhang, Boheng Zeng, Lianli Gao, Xianglong Liu, Jian Zhang, and Jingkuan Song. Frequency domain model augmentation for adversarial attack. In *European Conference on Computer Vision (ECCV)*, pages 549–566. Springer, 2022.
- [33] Nicholas A Lord, Romain Mueller, and Luca Bertinetto. Attacking deep networks with surrogate-based adversarial black-box methods is easy. In *International Conference on Learning Representations (ICLR)*, 2022.
- [34] Cheng Luo, Qinliang Lin, Weicheng Xie, Bizhu Wu, Jinheng Xie, and Linlin Shen. Frequency-driven imperceptible adversarial attack on semantic similarity. In *Proceedings of the IEEE/CVF Conference on Computer Vision and Pattern Recognition (CVPR)*, pages 15315–15324, 2022.
- [35] Aleksander Madry, Aleksandar Makelov, Ludwig Schmidt, Dimitris Tsipras, and Adrian Vladu. Towards deep learning models resistant to adversarial attacks. In *International Conference on Learning Representations (ICLR)*, 2018.
- [36] Dongyu Meng and Hao Chen. Magnet: a two-pronged defense against adversarial examples. In *Proceedings of the 2017 ACM SIGSAC Conference on Computer and Communications Security (ACM CCS)*, pages 135–147, 2017.
- [37] Seungyong Moon, Gaon An, and Hyun Oh Song. Parsimonious black-box adversarial attacks via efficient combinatorial optimization. In *International Conference on Machine Learning (ICML)*, pages 4636–4645. PMLR, 2019.
- [38] Seungyong Moon, Gaon An, and Hyun Oh Song. Preemptive image robustification for protecting users against man-in-the-middle adversarial attacks. In *Proceedings of the AAAI Conference on Artificial Intelligence (AAAI)*, pages 7823–7830, 2022.
- [39] Seyed-Mohsen Moosavi-Dezfooli, Alhussein Fawzi, and Pascal Frossard. Deepfool: a simple and accurate method to fool deep neural networks. In *Proceedings of the IEEE Conference on Computer Vision and Pattern Recognition (CVPR)*, pages 2574–2582, 2016.
- [40] Arkadij Semenovič Nemirovskij and David Borisovich Yudin. *Problem complexity and method efficiency in optimization*. Wiley-Interscience, 1983.
- [41] Yu Nesterov. Efficiency of coordinate descent methods on huge-scale optimization problems. *SIAM Journal on Optimization*, 22(2):341–362, 2012.
- [42] Maria-Irina Nicolae, Mathieu Sinn, Minh Ngoc Tran, Beat Buesser, Amrith Rawat, Martin Wistuba, Valentina Zantedeschi, Nathalie Baracaldo, Bryant Chen, Heiko Ludwig, Ian Molloy, and Ben Edwards. Adversarial robustness toolbox v1.2.0. *CoRR*, 2018.
- [43] Weili Nie, Brandon Guo, Yujia Huang, Chaowei Xiao, Arash Vahdat, and Animashree Anandkumar. Diffusion models for adversarial purification. In *International Conference on Machine Learning (ICML)*, pages 16805–16827, 2022.
- [44] Jeonghwan Park, Paul Miller, and Niall McLaughlin. Hard-label based small query black-box adversarial attack. In *Proceedings of the IEEE/CVF Winter Conference on Applications of Computer Vision (WACV)*, pages 3986–3995, 2024.
- [45] ShengYun Peng, Weilin Xu, Cory Cornelius, Matthew Hull, Kevin Li, Rahul Duggal, Mansi Phute, Jason Martin, and Duen Horng Chau. Robust principles: Architectural design principles for adversarially robust cnns. *arXiv preprint arXiv:2308.16258*, 2023.
- [46] Alec Radford, Jong Wook Kim, Chris Hallacy, Aditya Ramesh, Gabriel Goh, Sandhini Agarwal, Girish Sastry, Amanda Askell, Pamela Mishkin, Jack Clark, et al. Learning transferable visual models from natural language supervision. In *International conference on machine learning (ICML)*, pages 8748–8763. PMLR, 2021.
- [47] Edward Raff, Jared Sylvester, Steven Forsyth, and Mark McLean. Barrage of random transforms for adversarially robust defense. In *Proceedings of the IEEE/CVF Conference on Computer Vision and Pattern Recognition (CVPR)*, pages 6528–6537, 2019.
- [48] Min Ren, Yuhao Zhu, Yunlong Wang, and Zhenan Sun. Perturbation inactivation based adversarial defense for face recognition. *IEEE Transactions on Information Forensics and Security*, 17:2947–2962, 2022.
- [49] Hadi Salman, Andrew Ilyas, Logan Engstrom, Ashish Kapoor, and Aleksander Madry. Do adversarially robust imagenet models transfer better? *Advances in Neural Information Processing Systems (NeurIPS)*, 33:3533–3545, 2020.
- [50] Hadi Salman, Andrew Ilyas, Logan Engstrom, Sai Vemprala, Aleksander Madry, and Ashish Kapoor. Unadversarial examples: Designing objects for robust vision. *Advances in Neural Information Processing Systems (NeurIPS)*, 34:15270–15284, 2021.
- [51] Vikash Sehwal, Saeed Mahloujifar, Tinashe Handina, Sihui Dai, Chong Xiang, Mung Chiang, and Prateek Mittal. Robust learning meets generative models: Can proxy distributions improve adversarial robustness? In *International Conference on Learning Representations (ICLR)*, 2021.
- [52] Ali Shafahi, Mahyar Najibi, Amin Ghiasi, Zheng Xu, John Dickerson, Christoph Studer, Larry S Davis, Gavin Taylor, and Tom Goldstein. Adversarial training for free! In *Proceedings of the 33rd International Conference on Neural Information Processing Systems (NeurIPS)*, pages 3358–3369, 2019.
- [53] K Simonyan and A Zisserman. Very deep convolutional networks for large-scale image recognition. In *3rd International Conference on Learning Representations (ICLR)*. Computational and Biological Learning Society, 2015.
- [54] Naman D Singh, Francesco Croce, and Matthias Hein. Revisiting adversarial training for imagenet: Architectures, training and generalization across threat models. *arXiv preprint arXiv:2303.01870*, 2023.
- [55] Jiawei Su, Danilo Vasconcellos Vargas, and Kouichi Sakurai. One pixel attack for fooling deep neural networks. *IEEE Transactions on Evolutionary Computation*, 23(5):828–841, 2019.
- [56] Quoc Viet Vo, Ehsan Abbasnejad, and Damith Ranasinghe. Brusleattack: Query-efficient score-based sparse adversarial attack. In *The Twelfth International Conference on Learning Representations (ICLR)*, 2024.
- [57] Lina Wang, Kang Yang, Wenqi Wang, Run Wang, and Aoshuang Ye. Mgaattack: Toward more query-efficient black-box attack by microbial genetic algorithm. In *Proceedings of the 28th ACM International Conference on Multimedia (ACM MM)*, pages 2229–2236, 2020.
- [58] Qinglong Wang, Wenbo Guo, Kaixuan Zhang, Alexander G Ororbia, Xinyu Xing, Xue Liu, and C Lee Giles. Adversary resistant deep neural networks with an application to malware detection. In *Proceedings of the 23rd ACM SIGKDD International Conference on Knowledge Discovery and Data Mining (ACM SIGKDD)*, pages 1145–1153, 2017.

- [59] Yajie Wang, Yi Wu, Shangbo Wu, Ximeng Liu, Wanlei Zhou, Liehuang Zhu, and Chuan Zhang. Boosting the transferability of adversarial attacks with frequency-aware perturbation. *IEEE Transactions on Information Forensics and Security*, 19:6293–6304, 2024.
- [60] Zekai Wang, Tianyu Pang, Chao Du, Min Lin, Weiwei Liu, and Shuicheng Yan. Better diffusion models further improve adversarial training. In *International Conference on Machine Learning (ICML)*, pages 36246–36263. PMLR, 2023.
- [61] Zhibo Wang, Hengchang Guo, Zhifei Zhang, Wenxin Liu, Zhan Qin, and Kui Ren. Feature importance-aware transferable adversarial attacks. In *Proceedings of the IEEE/CVF International Conference on Computer Vision (ICCV)*, pages 7639–7648, 2021.
- [62] Zhou Wang, Alan C Bovik, Hamid R Sheikh, and Eero P Simoncelli. Image quality assessment: from error visibility to structural similarity. *IEEE Transactions on Image Processing*, 13(4):600–612, 2004.
- [63] Eric Wong, Leslie Rice, and J Zico Kolter. Fast is better than free: Revisiting adversarial training. In *International Conference on Learning Representations (ICLR)*, 2020.
- [64] Bichen Wu, Chenfeng Xu, Xiaoliang Dai, Alvin Wan, Peizhao Zhang, Zhicheng Yan, Masayoshi Tomizuka, Joseph Gonzalez, Kurt Keutzer, and Peter Vajda. Visual transformers: Token-based image representation and processing for computer vision. *arXiv preprint arXiv:2006.03677*, 2020.
- [65] Chenwang Wu, Wenjian Luo, Nan Zhou, Peilan Xu, and Tao Zhu. Genetic algorithm with multiple fitness functions for generating adversarial examples. In *2021 IEEE Congress on Evolutionary Computation (CEC)*, pages 1792–1799. IEEE, 2021.
- [66] Chaowei Xiao, Jun-Yan Zhu, Bo Li, Warren He, Mingyan Liu, and Dawn Song. Spatially transformed adversarial examples. In *International Conference on Learning Representations (ICLR)*, 2018.
- [67] Fei Yin, Yong Zhang, Baoyuan Wu, Yan Feng, Jingyi Zhang, Yanbo Fan, and Yujiu Yang. Generalizable black-box adversarial attack with meta learning. *IEEE Transactions on Pattern Analysis and Machine Intelligence*, 2023.
- [68] Richard Zhang, Phillip Isola, Alexei A Efros, Eli Shechtman, and Oliver Wang. The unreasonable effectiveness of deep features as a perceptual metric. In *Proceedings of the IEEE Conference on Computer Vision and Pattern Recognition (CVPR)*, pages 586–595, 2018.
- [69] Fei Zuo and Qiang Zeng. Exploiting the sensitivity of l2 adversarial examples to erase-and-restore. In *Proceedings of the 2021 ACM Asia Conference on Computer and Communications Security (ACM Asia CCS)*, page 40–51, 2021.

Appendix A.

User Study Questionnaire

We conducted user studies to assess the human perceptual visual quality of adversarial examples (AEs). In particular, we randomly selected 50 original images that were successfully attacked by six different methods, including the white-box AutoAttack [11], black-box GFCS [33] (for ImageNet), MCG [67] (for CIFAR-10), the sparse BruSLe attack [56], and our GreedyPixel under three distinct threat models. These attacks were executed on two datasets—CIFAR-10 (low-resolution images) and ImageNet (high-resolution images). For each dataset, we prepared a 50-question survey, as shown in Figure 9. To reduce bias towards specific attack methods, the test samples were presented in a random order. Participants were then asked to identify the AEs they considered visually indistinguishable from the original images.

Appendix B.

Evaluation Metrics

B.1. Attack Success Rate (ASR)

The ASR quantifies the effectiveness of an adversarial attack in altering the model’s prediction. It is defined as the proportion of AEs that successfully cause the model to produce incorrect predictions. Mathematically, it can be expressed as:

$$ASR = \frac{\text{Number of successful AEs}}{\text{Number of All AEs}}. \quad (12)$$

A higher ASR indicates a more effective attack, as it reflects the ability of the AEs to mislead the model.

B.2. Adversarial Detection Rate

The adversarial detection rate refers to the proportion of AEs that are correctly identified by an adversarial detector. It is defined as:

$$\text{Detection Rate} = \frac{\text{Number of AEs detected}}{\text{Number of All AEs}}. \quad (13)$$

A lower detection rate indicates higher attack efficacy, as it reflects the ability of the AEs to evade detection.

B.3. Structural Similarity Index (SSIM)

The SSIM is a metric for measuring similarity between two images. It considers luminance, contrast, and structural information. The SSIM between two images x (reference) and y (distorted) is defined as:

$$SSIM(x, y) = \frac{(2\mu_x\mu_y + C_1)(2\sigma_{xy} + C_2)}{(\mu_x^2 + \mu_y^2 + C_1)(\sigma_x^2 + \sigma_y^2 + C_2)}, \quad (14)$$

where:

- μ_x and μ_y : Mean intensity values of x and y , respectively.
- σ_x^2 and σ_y^2 : Variance of x and y , respectively.

- σ_{xy} : Covariance between x and y .
- C_1 and C_2 : Small constants added to stabilize the metric in the presence of weak denominators, defined as:

$$C_1 = (K_1L)^2, \quad C_2 = (K_2L)^2, \quad (15)$$

where L is the dynamic range of the pixel values (e.g., 255 for 8-bit images), and K_1 and K_2 are small positive constants (commonly, $K_1 = 0.01$ and $K_2 = 0.03$).

The SSIM value ranges from -1 to 1, where:

- 1: Perfect similarity.
- 0: No similarity.
- Negative values indicate dissimilarity.

SSIM is typically calculated locally using a sliding window across the image, and the overall SSIM is the average of local SSIM values. Higher SSIM values denote subtler deviations from the reference images.

B.4. Learned Perceptual Image Patch Similarity (LPIPS)

The LPIPS is a perceptual similarity measure that evaluates the perceptual distance between two images. It uses deep neural network features to compare the visual content and correlates better with human perception than traditional metrics like SSIM.

The LPIPS distance between two images x (reference) and y (distorted) is computed as:

$$LPIPS(x, y) = \sum_l \frac{1}{H_l W_l} \sum_{h=1}^{H_l} \sum_{w=1}^{W_l} w_l \|\hat{\phi}_l(x)_{h,w} - \hat{\phi}_l(y)_{h,w}\|_2^2, \quad (16)$$

where:

- l : Layer index in the deep network.
- $\phi_l(x)$: Feature map of x at layer l in the network.
- $\hat{\phi}_l$: Normalized feature maps for each channel.
- H_l, W_l : Height and width of the feature map at layer l .
- w_l : Learned scalar weights for each layer l (trained to match human judgments).

LPIPS uses a pretrained deep neural network to extract feature maps from intermediate layers. The metric normalizes the feature maps and computes the difference between them, weighted according to the learned weights w_l . The LPIPS value typically ranges from 0 (perfect perceptual similarity) to higher values indicating greater dissimilarity. LPIPS provides a perceptually grounded comparison, making it especially useful for evaluating subtle changes in visual quality.

User Study on Visual Quality of Adversarial Examples

Thank you for taking 10 minutes of your time to participate in this study.
Kindly provide your name and email address, and then select all the test images that have ****INVISIBLE**** differences from the original images.
Once your responses have been submitted, kindly send the log file to hanrui_wang@nii.ac.jp.
Important: Refreshing the page will reset all selections.

Question 40

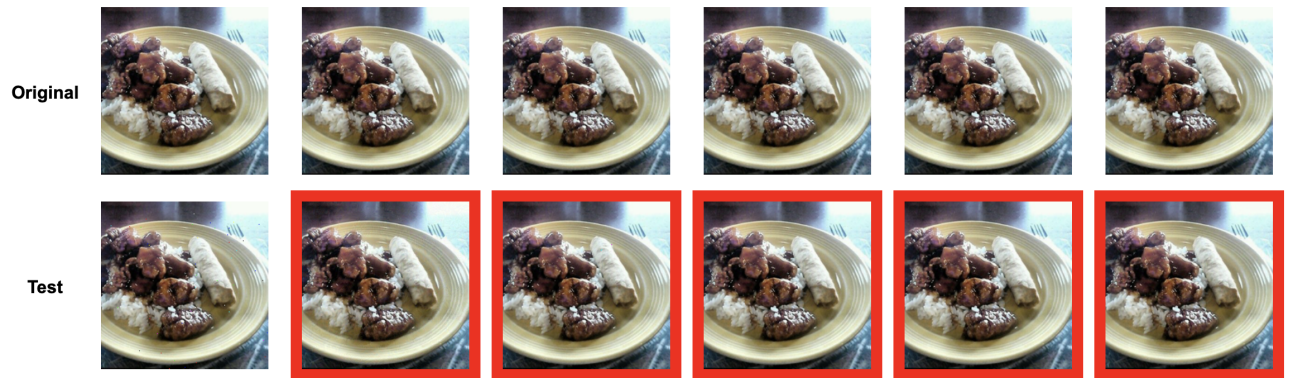


(a) CIFAR-10

User Study on Visual Quality of Adversarial Examples

Thank you for taking 10 minutes of your time to participate in this study.
Kindly provide your name and email address, and then select all the test images that have ****INVISIBLE**** differences from the original images.
Once your responses have been submitted, kindly send the log file to Anonymous.
Important: Refreshing the page will reset all selections.

Question 50



Submit

(b) ImageNet

Figure 9. The user study consisted of a 50-question questionnaire in which participants were asked to identify images they perceived to have no visible differences from the original counterparts. All images were derived from successful attacks generated by six distinct adversarial attack methods, including gradient-based AutoAttack [11], black-box GFCS [33] (for ImageNet) and MCG [67] attacks (for CIFAR-10), sparse BruSLe attack [56], and our GreedyPixel in three threat models as described in Table 4. The test samples were presented in randomized order. The test samples that the participants chose with imperceptible perturbations were enclosed in a red-bound square.